Journal of Solid State Chemistry 277 (2019) 61–67

Contents lists available at ScienceDirect

Journal of Solid State Chemistry

journal homepage: www.elsevier.com/locate/jssc

Thermodynamic study of $NaLaF_4$ in NaF-LaF_3 system using solid state electrochemical cell method

Sumanta Mukherjee [a,b,*], S. Dash [a,b]

[a] Fuel Chemistry Division
[b] Homi Bhabha National Institute (HBNI), Bhabha Atomic Research Centre, Trombay, Mumbai, 400085, India

ARTICLE INFO

Keywords:
$NaLaF_4$
Heat capacity
Gibbs free energy
SEGC
Phase diagram
Potential diagram

ABSTRACT

The NaF-LaF_3 system is characterized with single ternary fluoride compound, $NaLaF_4$. This compound has been synthesized in solid state route and characterized with X-ray diffraction technique. The purity has been checked with ICPMS technique. The heat capacity of $NaLaF_4$ (s) has been experimentally measured with differential Scanning Calorimeter and the variation of Cp as a function of temperature can be expressed as.

C_p /J.mol^{-1}K^{-1} = (171.2 ± 0.1) + (0.00089 ± 0.0002) × T/K - (3.235 × 10^6 ± 9204) × (T/K)$^{-2}$

The Gibbs energy of formation of $NaLaF_4$ (s) has been determined using Solid Electrolyte Galvanic Cell method with calcium fluoride as solid electrolyte. The $\Delta_f G$ of $NaLaF_4$ (s) as a function of temperature can be given as.

$\Delta_f G$ ($NaLaF_4$, s, T) (kJ mol^{-1}) = (- 2220.7 ± 0.7) + (0.3123 ± 0.0032) · (T/K)

Using the experimentally obtained thermodynamic data, the binary phase diagram of NaF (s) - LaF_3 (s) system has been calculated. To study the stability domain and coexisting phases of $NaLaF_4$(s), the chemical potential diagram of Na-La-F-O system and ternary phase diagram of Na-La-F system has been calculated.

1. Introduction

India has a large reservoir of thorium. The utilization of this thorium resource is one of the main aims of the third stage of the nuclear power program. In this stage the thorium can be used both in solid as well as liquid are Accelerator Driven System (ADS) and Indian Molten Salt Breeder Reactor (IMSBR) respectively. For sustainability of the third stage of the nuclear power program, the reactor system should have breeding ration of more than one, so, the reactor system should be a breeder system [1]. The IMSBR is expected to be more advantageous than the other reactor. The expected thermal efficiency of IMSBR will be also in the higher side [2]. In a typical molten salt reactor, the fuel {UF_4(s) +ThF_4(s)} is dissolved in molten fluoride salts of alkali and alkaline earth metals matrix circulating in the primary circuit from the reactor core to the heat exchanger and back [3-5].

The MSR is also designed as waste burner. In the waste, most of the actinides and lanthanides will be present as their trivalent fluoride compound. A binary mixture of {LiF-NaF} is an excellent suitable solvent for the trivalent actinide fluorides and lanthanide fluoride [6]. In the present work, thermodynamic study of the compound was carried out which might form due to high temperature interaction of NaF with lanthanum fluoride (LaF_3). It is observed that interaction of NaF with LaF_3 leads to form single ternary compound, $NaLaF_4$ (s). The existence of $NaLaF_4$ (s) in NaF (s) - LaF_3 (s) system has been described in literature [7, 8]. The details of the crystal structure of $NaLaF_4$ (s) has been studied by Thoma [9], Zachariasen [10] and Fedorov et. al. [11]. There is no experimental Gibbs energy of formation data available for the compound, $NaLaF_4$ in the literature. Though the binary phase diagram of NaF (s) - LaF_3 (s) system has been calculated earlier which are based on the estimated thermodynamic data. In the present study, the Gibbs energy of formation of $NaLaF_4$(s) has been experimentally measured using Solid Electrolyte Galvanic Cell (SEGC) with calcium fluoride as a solid electrolyte. The heat capacity of $NaLaF_4$(s) has been experimentally measured with Differential Scanning Calorimeter (DSC). Using the experimentally obtained thermodynamic data, the binary phase diagram of NaF (s) - LaF_3 (s) system has been calculated and the invariant points are compared with the previous work [6,12-14]. To study the stability domain and coexisting phases of $NaLaF_4$(s), the chemical potential diagram of Na-La-F-O system and ternary phase diagram of Na-La-F system has been calculated.

* Corresponding author.
E-mail address: sumantam@barc.gov.in (S. Mukherjee).

https://doi.org/10.1016/j.jssc.2019.05.037
Received 2 April 2019; Received in revised form 17 May 2019; Accepted 21 May 2019
Available online 28 May 2019
0022-4596/© 2019 Elsevier Inc. All rights reserved.

2. Experimental techniques

2.1. Materials

NaF (s) and LaF_3 (s) were used in the sample preparation. NaF(s) powder was procured from M/s Alpha Aesar, Germany whereas LaF_3 (s) has been synthesized indigenously by precipitation route. Stoichiometric amount of 40% HF (aq) was added to the aqueous solution of lanthanum nitrate, a white colour precipitate was formed. The precipitate was dried and characterized as LaF_3 (s). For e.m.f studies high purity nickel, iron, NiF_2 (s) and NiO (s) powders procured from LEICO Ind., New York were used for the preparation of electrodes. All the starting materials were subjected to pre-heat treatments at 473 K under inert argon flow to remove any residual moisture. The phase purity of the starting compounds was confirmed by X-ray analysis and was stored inside a glove box in argon atmosphere.

2.2. Synthesis and characterization of $NaLaF_4$(s)

$NaLaF_4$ (s) has been synthesized by solid state route. A homogeneous (1:1) mixture of NaF (s) and LaF_3 (s) was heated to 800°C in controlled argon atmosphere (Ar gas passed through three successive getter of molecular sieve-silica gel, uranium metal and potassium perchlorate for the removal of bulk moisture- oxygen, trace oxygen and trace moister respectively) through intermediate grinding and step heating of 200°C in each step.

The characterization of the sample was ascertained by powder X-ray powder diffraction (XRD) and the purity has been checked with ICPMS technique. The Powder XRD measurement of the sample was carried out on a Pan Analytical X-pert Pro diffractometer using Cu (Kα) ($\lambda = 1.5406$ Å) radiation and Ni filter. The operating conditions were 30 kV and 20 mA, in the 2θ range10-80°. The melting point of $NaLaF_4$ (s) has been determined by.

2.3. Measurements of heat capacity

The molar heat capacities of $NaLaF_4$ (s) were carried out using a heat flux-type differential scanning calorimeter (model number DSC 823°/700 of M/s. Mettler Toledo GmbH, Switzerland). For the measurement of $C^o_{p,m}(T)$, a classical three-step method [15] was used. The detail of the experiment was given in our previous work [16]. An average of three runs was carried out for heat capacity of $NaLaF_4$ (s).

2.4. Gibbs energy of formation: E.m.f. study

2.4.1. E m.f. (electromotive force) cell setup

In the present study the Gibbs energy of formation of $NaLaF_4$ (s) was also determined by E.m.f technique using single crystal CaF_2 electrolyte. For the measurement of E.m.f. the following electrochemical cell was used.

(Cell I) (-) Pt, 2 NaF(s) + La_2O_3 (s) + 2 $NaLaF_4$(s) |CaF_2 (s)| NiO (s)+ NiF_2(s), Pt (+) (1)

Here binary phase mixture of {NiO(s) + NiF_2(s)} was used as reference electrode and the three phase mixture: {2 NaF(s) + La_2O_3 (s) + 2 $NaLaF_4$(s)} was used as sample electrode. These electrodes were kept pressing against the two polished surface of the electrolyte (CaF_2) by a quartz holder and an alumina tube. The detailed of the fluoride cell is given in our previous study [17]. Prior to the e.m.f measurements, the E.m.f. cell assembly was validated and the co-existing phase field was established.

2.4.2. Establishment of equilibrium phase field

For the establishment of phase field, ternary phase mixture of dried NaF(s), La_2O_3(s), and $NaLaF_4$(s) contained in platinum crucibles was sealed in quartz ampoule under the dynamic vacuum of 10^{-6} mbar pressure. The ampoule was equilibrated at 900 K for 300 h and quenched to the room temperature.

2.4.3. Calibration of E.m.f cell setup

A single component cell setup was used for the E.m.f. measurements. Prior to the measurements, the E.m.f. cell assembly was calibrated employing the standard electrochemical cell:

(Cell II) (-) Pt, Fe(s) + FeF_2 (s)|CaF_2(s)| Ni(s)+ NiF_2(s), Pt (+) (3) (2)

The details of the calibration of the fluoride cell have been described in our previous work [18].

2.4.4. Preparation of electrodes

The ternary phase mixtures for sample electrode {NaF(s) + La_2O_3(s) + $NaLaF_4$(s)} and the reference electrode {NiO (s) + NiF_2(s)} were separately pelletized into cylindrical pellets of 10 mm diameter and 5 mm thickness for the e.m.f measurements. Then the sample and reference electrodes were made by attaching platinum discs to the palletized mixture of {NaF(s) + La_2O_3(s) + $NaLaF_4$(s)} and {NiO(s) + NiF_2(s)}, respectively.

3. Result and discussion

3.1. Characterization of $NaLaF_4$ (s)

The observed reflections of the powder XRD data was analyzed by comparing with its reported powder XRD pattern and was found to be in good agreement with the literature [JCPDS file no. 75-1923] XRD data [19]. No other XRD peak due to impurity phases including starting materials NaF and LaF_3 could be observed. The observed diffraction data was analyzed using Fullprof-2000 Rietveld refinement program [20] in which peak profile was fitted with Pseudo-Voigt profile function and U, V, W parameters were refined. In the initial stage the background parameters were adjusted with sixth order polynomial and appropriate scale factor. Rietveld refined XRD data for the compound $NaLaF_4$ is shown in Fig. 1. The derived cell parameters and residual parameters obtained from the refinement of XRD data for the compound is given in Table 1. The crystal structure of $NaLaF_4$ (s) which was drawn using VESTA program [21] using Rietveld refinement data was given in supplementary file (SF-1).

3.2. Impurity analysis

For the determination of trace elements which are present as impurities in $NaLaF_4$ (s), an inductively coupled plasma orthogonal

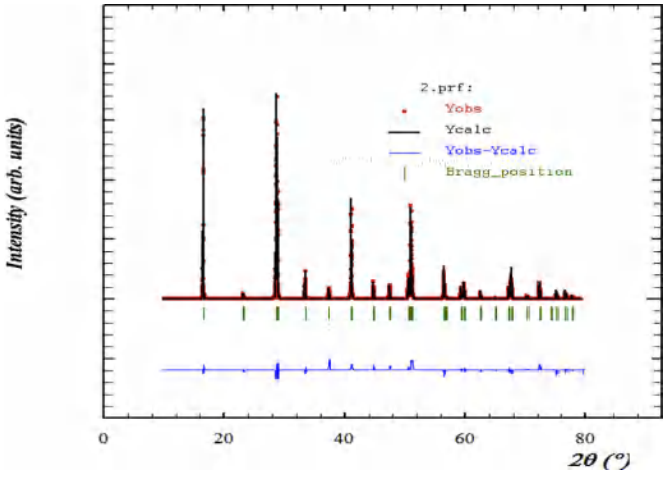

Fig. 1. Rietveld refined XRD pattern of $NaLaF_4$ (s).

Table 1
Refined structural parameters for $NaLaF_4$ (s).

a(Å)	b(Å)	c(Å)	α (°)	B (°)	γ (°)	V(Å^3)	U	V	W	χ^2	R_{exp}	Space Group
6.179866	6.179866	3.830958	90	90	120	126.7057	0.00389	0.007998	0.006255	1.51	10.31	P -6 (174)

acceleration time of flight mass spectrometer (ICP-oa-TOF-MS, Model Optimass 8000 R, GBC, Australia) was used. The ICPMS study show the high purity (~99.995%) of $NaLaF_4$ (s) as the impurity level is very less. Table 2 gives the detail of all impurity present in the compounds.

3.3. Melting point of $NaLaF_4$ (s)

The DTA curve for $NaLaF_4$ (s) was shown in Fig. 2. From the figure, the melting point of $NaLaF_4$ (s) has been found to be 1061 K. Here the onset temperature indicating the melting point of the compound.

3.4. Heat capacity of $NaLaF_4$ (s)

Heat capacity of $NaLaF_4$ (s) was measured in the temperature range 300–825 K. Three successive runs were carried out for the measurement of heat capacity. A temperature variation of C_p of $NaLaF_4$ (s) is shown in Fig. 3. The experimental molar heat capacity values were least square fitted to $C_p = A + B.T + C.T^{-2}$ equation. The expressions for the temperature dependent heat capacity in J.mol^{-1}K^{-1} of $NaLaF_4$ (s) is given by eq. (3).

$$C_p / \text{J.mol}^{-1}\text{K}^{-1} = (171.2 \pm 0.1) + (0.00089 \pm 0.0002) \times T/\text{K} - (3.235 \times 10^6 \pm 9204) \times (T/\text{K})^{-2} \quad (3)$$

Experimentally measured C_p of $NaLaF_4$ (s) and its comparison with Neumann-Kopp values (molar addition of C_p of NaF and LaF_3) is shown in Fig. 3 which also include the heat capacity of $NaLaF_4$ (s) given in the literature [6,13,22]. It shows that deviation of heat capacity of present study is within 1-11% obtained by F. Abdoun et al (experimental study) [13] and 1-24% obtained by van der Meer et al (obtained from assessment using polynomial model) [13]. Whereas the difference of C_p of present study and that measured by van der Meer et al [24] is 0.5 – 6%.

The positive deviation of the measured heat capacity of $NaLaF_4$ (s) was found which increases with temperature compared to the estimated heat capacity derived using Neumann-Kopp additive rule. Similar observation has been found in the literature [23] where the measured heat capacity was higher than the estimated value in case of complex fluoride system.

3.5. Establishment of equilibrium phase field

The XRD pattern of the equilibrated ternary mixture [containing NaF(s), La_2O_3(s), and $NaLaF_4$(s)] has been recorded and it does not show any new peak other than the starting material which indicate that at equilibrium {NaF(s), La_2O_3(s), and $NaLaF_4$(s)} were the co-existing phases which were used as sample electrode in the present study to find out Gibbs energy of formation of $NaLaF_4$(s). The XRD pattern of the equilibrium phase mixture (after heating) has been provided in supplementary figure (SF-2)

Table 2
Analyzed impurities in $NaLaF_4$ (s).

Elements	Concentration (ppm)	Elements	Concentration (ppm)
Al	5.231	Ni	0.663
Ba	6.175	Nd	0.662
Cr	21.000	Pb	1.622
Cu	20.875	Sr	30.001
Ce	1.175	Sc	1.113
Ga	0.526	Ti	0.485
Ge	1.616	V	2.023
Mo	2.113	W	59.523
Mg	0.898	Zn	2.052
Mn	22.751	Y	0.489
Nb	2.556		

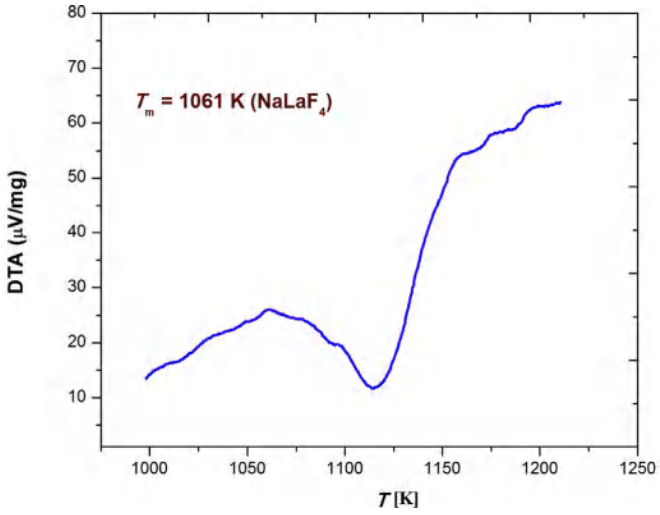

Fig. 2. DTA spectra of $NaLaF_4$ (s).

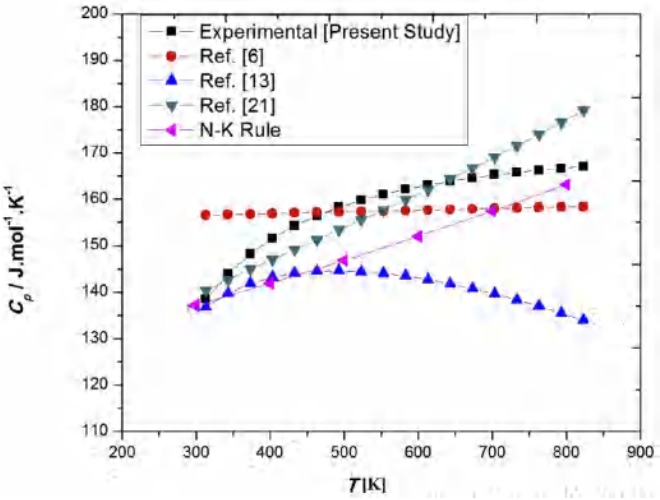

Fig. 3. Variation of heat capacity of $NaLaF_4$(s) with temperature.

3.6. Calibration

$$NiF_2\ (s) + Fe\ (s)\ FeF_2\ (s) + Ni\ (s) \quad (4)$$

The above equation is the reason for generation of E.m.f in the cell II (Eq. (2)).

Experimentally obtained E.m.f. values obtained from the cell II at different experimental temperature were expressed by a linear expression as given below:

$$E\ /\mathrm{V} \pm 0.0011 = 0.3108 + 2.55 \cdot 10^{-5} \cdot (T/\mathrm{K}) \quad (5)$$

The Gibbs energy of reaction of the net cell reaction (Eq. (4)) can be calculated from the relation:

$$\Delta_r G^o_m\ (T) = -\ \mathrm{n}.\ F.\ E \quad (6)$$

Where n is the number of electrons involved in the reaction, F is the faraday constant, F = 96484 C/Faraday.

$\Delta_r G^\circ_m\ (T)$ can be expressed as:

$$\Delta_r G^\circ_m\ (T)\ \{\pm 0.2\}\ \mathrm{kJ\ mol^{-1}} = -\ 59.9 + 4.92 \times 10^{-3}\ (T/\mathrm{K}) \quad (7)$$

The measured E.m.f.s (from eq. (5)) were used to calculate the Gibbs energy of formation of NiF_2 (s), $\Delta_f G^o_m(NiF_2,s,T)$ values and it is expressed as

$$\Delta_f G^o_m(NiF_2,s,T)\ \mathrm{kJ\ mol^{-1}} = (-642.9 \pm 0.2) + (0.1400 \pm 0.0003).\ T/\mathrm{K} \quad (8)$$

The $\Delta_f G^o_m(NiF_2,s,T)$ value calculated from Eq. (9) at 800 K, 900 K and 1000 K were found to be well matched with that reported by Barin [24] and the difference between the values are within 1%. It indicates that thermodynamic data generated by the cell is reliable.

3.7. Free energy of formation of $NaLaF_4$(s)

After the calibration the same experimental setup was used to determine the standard molar Gibbs energy of formation of $NaLaF_4$(s).

The E.m.f. was generated due to following cell reactions at anode and cathode of cell I.

At cathode

$$3\ NiF_2\ (s) + (3/2)\ O_2\ (g) + 6\ e^-\ 3\ NiO\ (s) + 6\ F^- \quad (9)$$

At anode

$$2\ NaF(s) + La_2O_3\ (s) + 6\ F^-\ NaLaF_4(s) + (3/2)\ O_2\ (g) + 6e^- \quad (10)$$

The net cell reaction is given as:

$$2\ NaF(s) + La_2O_3\ (s) + 3\ NiF_2\ (s)\ 2\ NaLaF_4(s) + 3\ NiO\ (s) \quad (11)$$

$$(-)\ Pt,\ 2\ NaF(s) + La_2O_3\ (s) + 2\ NaLaF_4(s)\ |CaF_2\ (s)|\ NiO\ (s) + NiF_2(s),\ Pt\ (+)$$

The variation plot of E.m.f. as a function of temperature has been seen in Fig. 4. From the plot, the linear expression of E.m.f. as a function of temperature was obtained and can be expressed as

$$E\ /\mathrm{V} = (0.4490 \pm 0.0014) + (5.66 \pm 0.31) \times 10^{-5}.\ (T/\mathrm{K}) \quad (12)$$

From Eq. (12), the Gibbs energy of reaction of the net cell reaction has been calculated using the equation $\Delta_r G^o_m(T) = -\ \mathrm{n}.\ F.\ E$ (here n = 6) and can be expressed as

$$\Delta_r G^\circ_m\ (T)\ \mathrm{kJmol^{-1}} = (-259.9 \pm 0.8) - (0.0327 \pm 0.0021).\ (T/\mathrm{K}) \quad (13)$$

For the net cell reaction the Gibbs energy of reaction can be expressed as

$$\Delta_r G\ (T) = 2.\ \Delta_f G\ (NaLaF_4,\ s,\ T) + 3.\ \Delta_f G\ (NiO,\ s,\ T) - 2.\ \Delta_f G\ (NaF,\ s,\ T) - \Delta_f G\ (La_2O_3,\ s,\ T) - 3.\Delta_f G\ (NiF_2,\ s,\ T \quad (14)$$

$$2.\ \Delta_f G\ (NaLaF_4,\ s,\ T) = 3.\ \Delta_f G\ (NiO,\ s,\ T) - 2.\ \Delta_f G\ (NaF,\ s,\ T) - \Delta_f G\ (La_2O_3,\ s,\ T) - 3.\ \Delta_f G\ (NiF_2,\ s,\ T) - \Delta_r G\ (T) \quad (15)$$

$$\Delta_f G\ (NaLaF_4,\ s,\ T) = (1/2)\ [3.\ \Delta_f G\ (NiO,\ s,\ T) - 2.\ \Delta_f G\ (NaF,\ s,\ T) - \Delta_f G\ (La_2O_3,\ s,\ T) - 3.\ \Delta_f G\ (NiF_2,\ s,\ T) - \Delta_r G\ (T)] \quad (16)$$

The value of $\Delta_f G\ (NaLaF_4,\ s,\ T)$ can be obtained by incorporating the value of $\Delta_f G\ (NiO,\ s,\ T)$, $\Delta_f G\ (NaF,\ s,\ T)$, $\Delta_f G\ (La_2O_3,\ s,\ T)$ and $\Delta_f G\ (NiF_2,\ s,\ T)$ from literature and value of $\Delta_r G\ (T)$ from Eq. (13). The $\Delta_f G\ (NaLaF_4,\ s,\ T)$ can be expressed as:

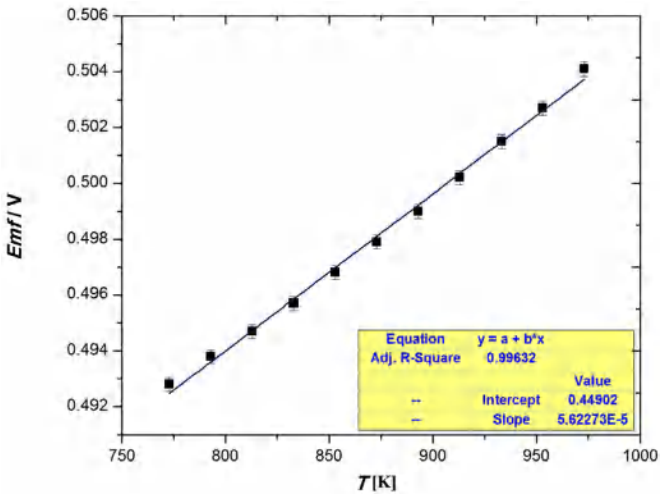

Fig. 4. Variation of E.m.f with temperature for the cell.

$$\Delta_f G\ (NaLaF_4,\ s,\ T)\ (\mathrm{kJ\ mol^{-1}}) = (-\ 2220.7 \pm 0.7) + (0.3123 \pm 0.0032) \cdot (T/\mathrm{K}) \quad (17)$$

The standard molar enthalpy and entropy of formation of $NaLaF_4$(s) at 298 K derived using second law and third law method and were found to be -2242.2 kJ mol^{-1} and 169.7 J $mol^{-1}K^{-1}$ respectively. The details of "second law and third law method", for calculation of the thermodynamic parameters are given below. The detail calculation technique has been given by M. W. Chase [25].

4. Construction of thermodynamic tables for $NaLaF_4$ (s)

The thermodynamic functions for $NaLaF_4$(s) were calculated using following relations.

$$H^o_m(T) - H^o_m(298.15) = \int_{298.15}^{T} \left(C^o_{p,m}\right) dT \quad (18)$$

$$S^o_m(T) = S^o_m(298.15) + \int_{298.15}^{T} \left(\frac{C^o_{p,m}(T)}{T}\right) dT \quad (19)$$

$$-\left(\frac{\left(G^o_m(T) - H^o_m(298.15)\right)}{T}\right) = S^o_m(T) - \frac{\left(H^o_m(T) - H^o_m(298.15)\right)}{T} \quad (20)$$

$$\Delta_f G^0_m(T) = \Delta_f H^0_m(T) - T\ \Delta_f S^0_m(T) \quad (21)$$

The enthalpies of formation at 298.15 K, $S^o_m(NaLaF_4,\ s,\ 298.15\ \mathrm{K})$ and heat capacities of $NaLaF_4$(s) determined in this study have been used in Eq. 18–21, for the computation of thermodynamic table. The resulted thermodynamic functions for $NaLaF_4$ (s) are given in Table 3.

5. Ternary phase diagram of Na-La-F system

In this study, FTSalt and newly generated databases has been used for the solid and liquid solutions of Na-La-F system using the Factsage software [26].

The ternary phase diagram of Na-La-F system was calculated by minimization of Gibbs energies of phases present in Na-F, La-F, La-Na and La-Na-F systems. La-F system [24] has a single fluoride compound, LaF_3 in condensed and liquid phase. Na-F system also has a single binary fluoride compound, NaF in condensed phase, liquid phase and gaseous phase. No compound is reported in Na-La system. The required input data

Table 3
Thermodynamic functions for $NaLaF_4$ (s).

T/K	C_p (T) J.K^{-1}.mol^{-1}	$S^o_m(T)$ J.K^{-1}.mol^{-1}	$H_m(T)$ - $H_m(298)$ kJ.mol^{-1}	Fef [Φ] J.K^{-1}.mol^{-1}
298	135.1	169.7	0	169.6
300	135.5	170.5	0.3	169.7
350	145.1	192.2	7.2	171.4
400	151.3	212.0	14.7	175.3
450	155.6	230.1	22.8	180.4
500	158.7	246.6	30.2	186.2
550	160.9	261.9	38.2	192.4
600	162.7	275.9	46.3	198.7
650	164.1	289.1	54.5	205.2
700	165.2	301.3	62.7	211.6
750	166.1	312.7	71.0	218.0
800	166.8	323.5	79.4	224.3
850	167.5	333.6	87.7	230.4
900	168.0	343.2	96.1	236.4
950	168.5	252.3	104.5	242.3
1000	168.8	360.9	112.9	247.9

Fef [Φ]: Free energy function, $fef = -[G_m(T)-H_m(298)]/T$.

for the Factsage software [26] were taken from the FactPS database and thermochemical tables of Barin [24] and that for $NaLaF_4$ (s) was taken from this study.

The average operating temperature of the MSR is above 775 K. So at that reactor operating condition, to study the coexisting phases and stability of different compounds the ternary phase diagram of Na-La-F system has been calculated at 800 K and 1 bar which is shown in Fig. 5. It shows that $NaLaF_4$ (s) co-exists with La (s), NaF (s), LaF_3(s) and F_2(g).

6. Binary phase diagram of NaF (s)-LaF_3 (s) system

The Gibbs energy of formation of phases of Na-F, La-F, La-Na and Na-La-F are required to calculate the pseudo binary phase diagram of {NaF - LaF_3} system.

The Gibbs energy of NaF- LaF_3 solution phase [27,28] can be expressed as:

$$G^{sol}(T) = x_{NaF}\, G^o(NaF,T) + x_{LaF3} G^o(LaF_3,T) + R \cdot T\,(x_{NaF} \ln x_{NaF} + x_{LaF3} \ln x_{LaF3}) + G^{ex} \quad (22)$$

The excess contribution to the Gibbs energy is the only unknown term in the above expression and also responsible for the deviation between the ideal and the real systems. The determination of the unknown excess Gibbs energy is very important for further calculation. In this study, liquid solution is described using the classical polynomial model in which the excess Gibbs energy [28,29] is defined as

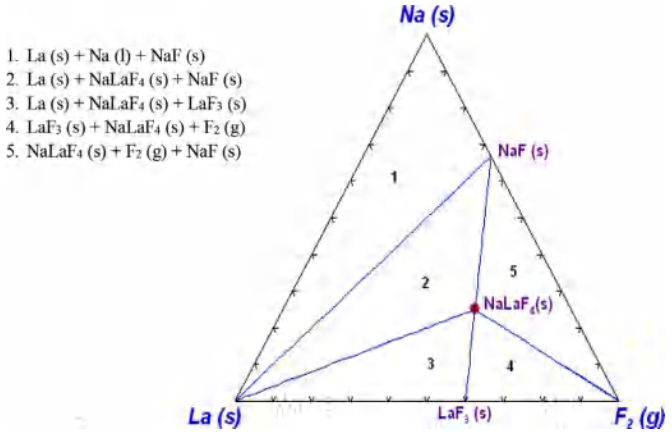

Fig. 5. Ternary phase diagram of Na-La-F System at 800 K.

$$G^{ex} = \sum_{ij} x_{(NaF)} \cdot x_{(LaF3)} L_{ij} \quad (23)$$

The interaction term $L_{i,j}$ could be described as a function of temperature with the general equation as

$$L_{i;j} = A + B.T + C.T \ln T + dT^2 \quad (24)$$

The parameters of the above equation (A, B, C, D…) were optimized during the thermodynamic assessment of experimental and calculated data. The classical polynomial model was used to describe the (Na, La)F_x liquid. The coefficients of the interaction parameters were calculated by two main routes, the first path is trial and error approach and second path is mathematical iteration. In the first path, the selection of the values of the coefficients was based on experiences but the process was arbitrary and afterwards they were refined. In this case, the polynomial was kept as simple as possible. In the second path, the coefficients were calculated using mathematical iteration. Both methods were used to calculate G^{ex} values. The binary phase diagram of NaF- LaF_3 system was calculated by the phase diagram module of the programme [26]. The calculated NaF-LaF_3 phase diagram is a peritectic system and shown in Fig. 6. The exact temperatures of the peritectic and eutectic point are mentioned in Table 4 and compared with literature [6,12-14]. Fig. 6 shows that $NaLaF_4$(s) is stable from room temperature up to 1061 K, where it melts peritectically. The eutectic point of the system has a composition of 28 mol % LaF_3 and 72 mol % NaF at 1011 K.

7. Chemical potential diagram of Na-La-F-O system

In this type of diagram, the phases of Na-La-F-O system has been plotted as a function of log ($p(F_2)$) along y-axis and log($p(O_2)$) along x-axis. For this four component systems at constant pressure and temperature, three phases coexist at F=0, two phases coexist at F=1 and a single phase is stable for F=2. In order to compute the stability domain of $NaLaF_4$ (s) in presence of oxygen impurity, the chemical potential diagram of Na-La-F-O systems have been computed at 800 K, shown in Fig. 7. The potential diagrams were calculated based on the Gibbs energy minimization technique. The detail technique of calculation of the

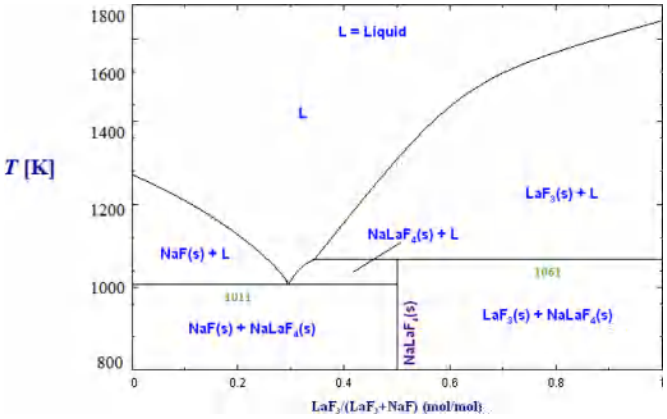

Fig. 6. Binary phase diagram of NaF(s)-LaF_3(s) System.

Table 4
Comparison of eutectic and Peritectic point with previous work.

Temperature (K)	van der Meer et. al. [6].	O. Benes et. al. [14].	R. E. Thoma et. al. [12].	F. Abdoun et. al. [13].	Present Study
Eutectic Point	1011.5	1008	1003	1008	1011
Peritectic Point	1054.6	1058	1083	1054	1061

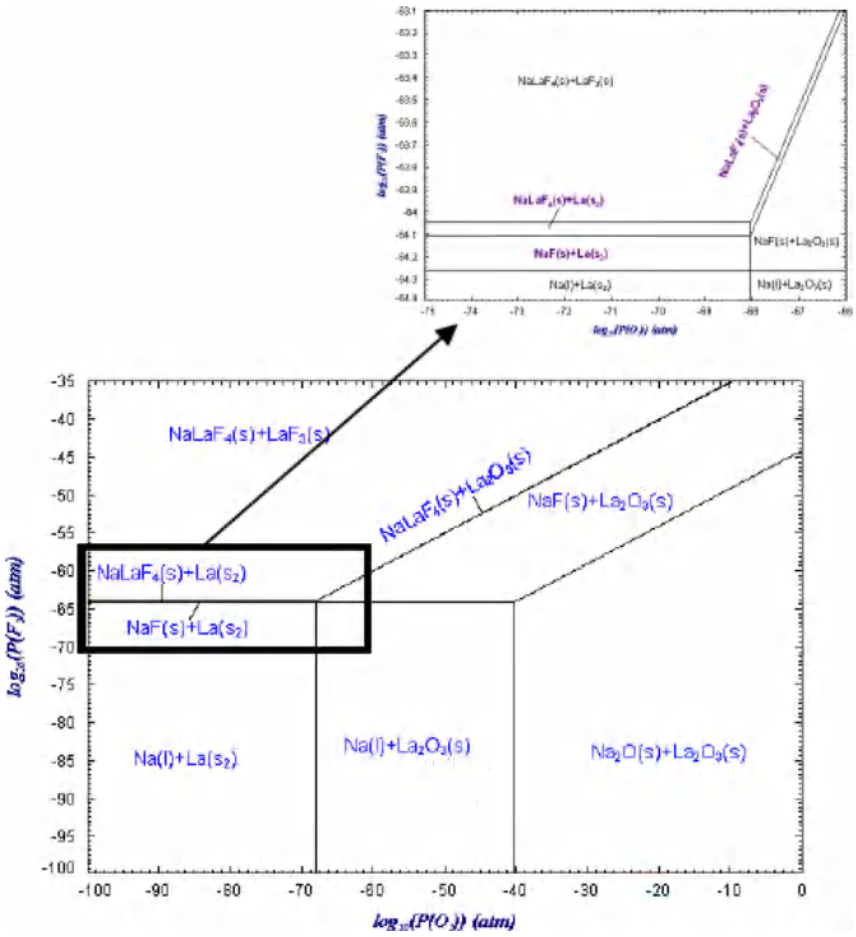

Fig. 7. Chemical potential Diagram of Na-La-F-O System at 800 K.

potential diagram was given in our previous work [30]. The required Gibbs energy data of unary and binary compounds in Na-La, La-F, F-O, Na-F, La-O and Na-O systems have been taken from the literature [18].The required Gibbs energy data of the ternary compounds in Na-La-F system has been experimentally determined in our present study and for other ternary systems, the required Gibbs energy data of the ternary compounds, have been taken from literature.

The potential diagrams show that with increasing temperature the stability domain of binary phase, {$NaLaF_4$ (s) + LaF_3 (s)} decreases with increase in temperature. Apart from this the potential diagram also shows that $NaLaF_4$ (s) coexist with La_2O_3 (s), LaF_3 (s) and La (s). The potential diagram indicates that with increase in temperature the required fluorine pressure for formation of $NaLaF_4$ (s) will also increase.

8. Conclusions

$NaLaF_4$ (s) is the only compound which form due to the high temperature interaction of NaF (s) and LaF_3 (s). $NaLaF_4$ (s) has been synthesized by solid state route. The characterization and impurity analysis of this compound has been done with XRD technique and ICP-MS respectively. The Gibbs energy of formation of $NaLaF_4$ (s) has been measured using solid electrolyte Galvanic cell and the heat capacity also measured with differential scanning calorimeter for the first time. The experimental heat capacity shows higher values compare to the estimated value which was calculated by N-K rule. The standard molar enthalpy and entropy of formation of $NaLaF_4$(s) at 298 K derived using second law and third law method and were found to be -2242.2 kJ mol^{-1} and 169.7 J $mol^{-1}K^{-1}$ respectively. Using the experimental thermodynamic data the thermodynamic table for $NaLaF_4$ (s) has been calculated. The binary phase diagram of NaF(s) - LaF_3(s) system has been calculated which shows that $NaLaF_4$(s) is stable from room temperature up to 1061 K, where it melts peritectically. The eutectic point of the system has a composition of 28 mol % LaF_3 and 72 mol % NaF at 1011 K. The ternary phase diagram of Na-La-F system shows that shows that $NaLaF_4$ (s) coexists with La (s), NaF (s), LaF_3(s) and F_2(g). The stability domain of $NaLaF_4$ (s) has been studied by calculating the isothermal chemical potential diagram of Na-La-F-O system at 800 K.

Acknowledgements

The authors are thankful to Dr. S. Kannan, Head, Fuel Chemistry Division, for his constant support and encouragement. The authors are also thankful to Shri Buddhadev Kanrar and Shri. Muhammed Shafeeq P P for X-Ray Diffraction Analysis of the samples.

Appendix A. Supplementary data

Supplementary data to this article can be found online at https://doi.org/10.1016/j.jssc.2019.05.037.

References

[1] P.K. Vijayan, A. Basak, I.V. Dulera, K.K. Vaze, S. Basu, R.K. Sinha, Pramana - J. Phys. 85 (3) (2015) 539–554.
[2] R.K. Sinha, Energy Procedia 7 (2011) 34–50.
[3] A technology roadmap for generation IV nuclear energy systems", U. S. DOE Nucl. Energy Res. Advis. Comm. Generat. IV Int. Forum 39 (2002).
[4] P. R. Kasten, "Safety Program for Molten-Salt Breeder Reactors," ORNL-TM-1858, Oak Ridge National Laboratory (June 9, 1967)
[5] E. McCoy and J.R. Weir, "Materials Development for Molten Salt Breeder Reactors," ORNL-Tm1854, Oak Ridge National Laboratory (June 1967)

[6] J.P.M. van der Meer, R.J.M. Konings, K. Hack, H.A.J. Oonk, Chem. Mater. 18 (2006) 510–517.
[7] F. Matthes, S. Holz, Z. Chem. 2 (1962) 22.
[8] G.A. Bukhalova, E.P. Babaeva, T. M Khliyan, Russ. J. Inorg. Chem. (Engl. Transl.) 10 (1965) 1158–1164.
[9] R.E. Thoma, Proc. Fourth Rare Earth Research Conference, Phoenix, AZ, 1964, p. 22.
[10] W.H. Zachariasen, J. Am. Chem. Soc. 70 (1948) 2147–2153.
[11] P.P. Fedorov, I.I. Buchinskaya, O.S. Bondareva, A.A. Bystrova, S.P. Ivanov, V.A. Stasyuk, B.P. Sobolev, L.L. Vistin', D.A. Ershov, J. Inorg. Chem. 45 (2000) 949–952 (translated from *Zhurnal Neorganicheskoi Khimii*).
[12] R.E. Thoma, H. Insley, G.M. Hebert, Inorg. Chem. 5 (7) (1966) 1222–1229.
[13] F. Abdoun, M. Gaune-Escard, G. Hatem, J. Phase Equilibria 18 (1) (1997) 6–20.
[14] O. Benės, J.P.M. van der Meer, R.J.M. Konings, Calphad Comput. Coupling Phase Diagrams Thermochem. 31 (2007) 209–216.
[15] G.W.H. Hohne, W.F. Hemminger, H.J. Flammershein, Differential Scanning Calorimetry, second ed., Springer, Berlin, 2003.
[16] S. Mukherjee, S. Dash, J. Solid State Electrochem. 23 (2019) 307–314.
[17] S. Mukherjee, S. Dash, J. Fluorine Chem. 212 (2018) 17–25.
[18] S. Mukherjee, S. Dash, S.K. Mukerjee, K.L. Ramakumar, J. Nucl. Mater. 465 (2015) 604–614.
[19] PDF-2 Database, Powder Diffraction File, International Centre for Diffraction Data, Pennsylvania, 1997.
[20] J. Rodriguez-Carvajal, Fullprof 2000 Version 1.6, Laboratoire Leon Brillouin, Gifsur Yvette, France, 2000.
[21] K. Momma, F. Izumi, VESTA 3 for three-dimensional visualization of crystal, volumetric and morphology data, J. Appl. Crystallogr. 44 (2011) 1272–1276.
[22] J.P.M. van der Meer, R.J.M. Konings, D. Sedmidubsky, A.C.G. van Genderen, H.A.J. Oonk, J. Chem. Thermodyn. 38 (2006) 1260–1268.
[23] O. Beneš, R.J.M. Konings, C. Kuenzel, M. Sierig, A. Dockendorf, L. Vlahovic, J. Chem. Thermodyn. 41 (2009) 8993.
[24] I. Barin, O. Knacke, Thermochemical Properties of Inorganic Substances, Springer - Verlag, New York, 1973.
[25] M.W. Chase Jr., C.A. Davies, J.R. Downey Jr., D.J. Fruip, V. McDonald, A.N. Syverud, J. Phys. Chem. Ref. Data 14 (1) (1985) 14–15. Monograph 9, JANAF Thermochemical Tables, 1995 (4th Ed.).
[26] Version 6 FactSage, 3, "The Integrated Thermodynamic Data Bank System", GTT Technologies, GmbH, Germany, 1976–2006.
[27] H.L. Lukas, S.G. Fries, B. Sundman, Computational Thermodynamics, the Calphad Method, Cambridge University Press, 2007.
[28] L. Kaufman, H. Bernstein, Computer Calculation of Phase Diagrams, Academic Press, New York, 1970.
[29] A.D. Pelton, P. Chartrand, G. Eriksson, Metall. Mater. Trans. A 32A (6) (2001) 1409–1416.
[30] S. Mukherjee, S. Dash, J. Radioanal. Nucl. Chem. 313 (2017) 497–504.